Journal of Magnetism and Magnetic Materials 125 (1993) 78–90
North-Holland

journal of magnetism and magnetic materials

The microstructural characterisation of Nd–Fe–B alloys. I: Light element microanalysis

X.J. Yin [1], M.G. Hall, I.P. Jones, R.N. Faria and I.R. Harris

School of Metallurgy and Materials, University of Birmingham, Birmingham B15 2TT, UK

Received 22 June 1992

Analyses of oxygen and boron with spatial resolutions of a few μm have been carried out using wavelength dispersive X-ray spectrometry (WDX) in a SEM on an as-cast $Nd_{15}Fe_{77}B_8$ alloy (annealed at 1100°C for 1 h, followed by furnace cooling) and a laboratory produced [hydrogen decrepitation (HD) route] $Nd_{16}Fe_{76}B_8$ sintered magnet. The optimum experimental parameters including standards, accelerating voltage and analysing crystal were determined. Excellent apparent concentration reproducibility has been achieved. Area/peak factors (APFs) for boron K for the $Nd_2Fe_{14}B$ matrix phase and $Nd_{(1+\epsilon)}Fe_4B_4(\epsilon \sim 0.1)$ boron-rich phase have been determined with a Pb stearate crystal on a JEOL 840A SEM relative to a pure boron standard. The integral intensity ratios were corrected using both the commercial LINK on-line ZAF-4 (FRAME-C) programme and the COR-2 programme. Probably the best accuracy of boron measurements has been achieved by use of APFs and the COR-2 programme (equipped with Heinrich's mass absorption coefficients). In contrast, the boron results (pure boron standard) from the on-line ZAF-4 programme are much higher than the reported stoichiometric concentration of the matrix and the boron-rich phase, although this has been improved by the use of an FeB standard. The mass absorption coefficient for oxygen absorbed by Nd derived from pure Nd_2O_3 powder using the convergent beam technique (for thickness determination) and ultra-thin window EDX on a TEM is reasonably close to Heinrich's and Henke's values. The results show that the triple junction regions and the $Nd_2Fe_{14}B$-$Nd_2Fe_{14}B$ grain boundaries contain the Nd-rich phase with Nd: ~90 at%, Fe: ~1 at%, oxygen: 8–9 at% and boron: <1 at%. Auger spectroscopy results show that the oxygen present in the matrix phase and in the boron-rich phase exists only in the surface layer. By contrast the oxygen reacted with the Nd-rich boundary phase to form a bulk oxide.

1. Introduction

Permanent magnets based on Nd–Fe–B alloys are prepared typically by a powder metallurgy sintering process. Oxygen is present in the initial alloys and more is introduced during milling and subsequent processing. The magnetic properties of the sintered magnets, especially the coercivity, depend sensitively on the oxygen content. Thus a detailed knowledge of the oxygen content is an important aid to processing, and quantitative measurements of boron are also important in providing valuable information on the phase compositions in these boron-containing materials.

Compared with conventional analysis of medium to high-Z elements ($Z > 11$), successful analysis of light elements requires far more care. Techniques for analysis of boron and oxygen with a spatial resolution of less than a few μm, are shown in table 1.

The energy resolution of WDX is better than that of EDX. Since this improvement in resolution results in a better peak/background ratio, the detectability limit is better: ~0.01% for normal elements and ~0.1% for light elements [1].

The conversion of apparent concentrations ($k = I_{\text{specimen}}/I_{\text{std}}$ intensity ratio) into true concentrations constitutes the well known 'ZAF' correc-

Correspondence to: Dr I.P. Jones, School of metallurgy and Materials, University of Birmingham, Birmingham B15 2TT, UK.

[1] *Present address*: Metals and Advanced Materials Centre, Singapore Institute of Standards and Industrial Research, 1 Science Park Drive, Singapore 0511.

0304-8853/93/$06.00 © 1993 – Elsevier Science Publishers B.V. All rights reserved

tions ($F = F_a F_f F_b F_s$). These include: (1) F_a, absorption of characteristic X-rays emerging from the specimen; (2) F_f, enhancement of the characteristic X-ray intensity due to fluorescence by other lines and the X-ray continuum; (3) F_b, loss of X-ray intensity owing to incident electrons being backscattered out of the specimen; and (4) F_s, variation in the efficiency of X-ray production, which is governed by the 'stopping power' of the specimen (a function of atomic number) [2]. However, it is well known that for light elements the peak position and shape change significantly, depending upon the type of the chemical bond involved. Therefore, with very light elements it can be misleading to measure X-ray intensities at the position of the maximum of the emission peaks [3–5]. There are many computer programmes for performing ZAF corrections which are available today, for example the ZAF-4 (based on the FRAME-C [6]) programme (Oxford Instruments Ltd) and the COR-2 programme [7]. In this study, both programmes were employed and compared. For the light elements, absorption is usually the major correction and, unfortunately, any correction procedure is faced with the fact that the mass absorption coefficients for soft X-rays are known only with limited accuracy. A novel idea for measuring mass absorption coefficients has emerged from this investigation.

Bastin and Heijligers [8] carried out an interesting experiment with a new multilayer LDE crystal to detect an oxygen peak on pure gold. They suggested that oxygen contamination is almost as bad a problem as carbon contamination, and the former effect is much more difficult to allow for than the latter. Therefore, in the present work, Auger spectroscopy was employed to examine the surface concentrations of oxygen and boron.

2. Experimental work

The samples chosen for this investigation were an as-cast $Nd_{15}Fe_{77}B_8$ ingot and a $Nd_{16}Fe_{76}B_8$ sintered magnet. The cast $Nd_{15}Fe_{77}B_8$ ingot was supplied by Rare-Earth Products plc, and was homogenised at 1100°C for 1 h, followed by furnace cooling to room temperature. The sintered $Nd_{16}Fe_{76}B_8$ magnet was produced by the hydrogen decrepitation (HD) route described by Harris [9]. The magnetic properties were measured using a permeameter.

After mounting with FeB standards, the specimens were ground and polished. The microstructures of the specimens were observed by SEM.

WDX was used to investigate the boron and oxygen concentrations in the Nd–Fe–B samples. Due to the reactivity of these materials, any non-recently prepared specimens would have excess surface oxidation. All the specimens were therefore repolished very carefully immediately prior to each WDX measurement. Peaks were corrected for background and for the oxygen measurements, a SiO_2 standard was used and for the boron measurements, pure boron and FeB standards were employed. Areas of peaks were produced by slowly scanning the range around the boron peak with the WDX spectrometry. The true peak area was found by adding the channels beneath the peak and subtracting the background.

Pure Nd_2O_3 powder was provided by Rare-Earth Products plc. The powders were suspended

Table 1

Technique [a]	Approximate resolution	Comments
WDX on SEM	1 μm	Accurate boron analysis
Auger	1 μm	Imaging not good. Good for surface analyses
UTW EDX (TEM)	10 nm	Currently not quantitative
STEM + EELS	10 nm	Low sensitivity; difficult to quantify

[a] WDX, wavelength dispersive X-ray spectrometry; SEM, scanning electron microscope; Auger, Auger electron spectroscopy; UTW EDX, ultra-thin window energy dispersive X-ray spectrometry; STEM, scanning transmission electron microscopy; EELS, electron energy loss spectroscopy.

Fig. 1. Secondary electron image (tilt = 0°) of a polished cast $Nd_{15}Fe_{77}B_8$ sample on a JEOL 840A SEM. (a) matrix phase, (b) Nd-rich phase and (c) boron-rich phase.

in methanol, picked up by copper grids with a thin carbon film and then put into a JEOL 4000FX TEM such that the powder sitting on the thin carbon film was exposed to the incident electron beam. The thicknesses of the Nd_2O_3 powder particles were measured by the convergent beam technique [10] and the X-ray spectra were collected at the same time by ultra-thin window EDX on a JEOL 4000FX TEM. The background Bremsstrahlung was subtracted from the spectra by offsetting the cursor on either side of the peaks so that the relative intensities of the characteristic X-rays could be determined.

VG Auger spectroscopy was used to investigate qualitatively the surface concentrations of oxygen and boron. Auger spectra are obtained generally in the form of a differentiated graph. Qualitative analysis can be achieved by the comparison of peak energy values and peak shapes of differentiated Auger spectra with those from standard specimens, which are available in handbooks. Depth profiling was carried out by Ar ion sputtering (probe current 0.4 mA) for 15 min. The filament current, emission current, probe current and beam voltage were 2.5 A, 0.1 mA, 10 nA and 10 kV, respectively.

3. Results

3.1. Microstructures and magnetic properties

Figure 1 shows a secondary electron scanning micrograph of the cast $Nd_{15}Fe_{77}B_8$ alloy, which

Table 2
Magnetic properties of sintered $Nd_{16}Fe_{76}B_8$

Sample	B_r (kG)	${}_iH_c$ (kOe)	${}_bH_c$ (kOe)	$(BH)_{max}$ (MGOe)	Squareness factor	Density (g/cc)
Sintered $Nd_{16}Fe_{76}B_8$ (HD route)	12.26 ±0.01	12.72 ±0.03	11.31 ±0.06	38.24 ±0.21	0.90	7.457 ±0.001

was annealed at 1100° for 1 h, followed by furnace cooling. It exhibits three phases: the hard magnetic matrix phase (a), the intergranular Nd-rich phase (b) and the boron-rich phase (c). The domains in the matrix phase are displayed clearly. The origin of this domain contrast has been discussed elsewhere [11].

The magnetic properties of the laboratory produced sintered $Nd_{16}Fe_{76}B_8$ magnet are shown in table 2. The microstructure of the sintered $Nd_{16}Fe_{76}B_8$ magnet was studied by SEM (fig. 2), which revealed a morphology consisting of the majority matrix grains, the Nd-rich phase and the boron-rich phase.

3.2. EPMA results

3.2.1. Experimental parameters

Accelerating voltage. With an increase in accelerating voltage (e.g. up to 20 kV), the generation depth of X-rays becomes large and absorption levels are very high for light elements. The improvement in the light element measurements obtainable by reducing the accelerating voltage E_0 is limited ultimately by the need to have $E_0 \gg E_c$ (critical excitation energy). Reducing the accelerating voltage (e.g. to 5 kV), however, increases the diameter of the beam probe and results in poor spatial resolution. A compromise 10 kV accelerating voltage was therefore employed in the present studies.

Crystal selection. A synthetic crystal (LDE-1) was used for oxygen and a Pb stearate crystal (STE) for boron.

Cold finger. A cold 'finger' was placed close to the specimen where it reduced the local partial pressure of the residual vapours in the system and, thus, contamination.

Quantitative analysis. An apparent concentration (k): $k = I_{sample}/I_{std} = (Peak - Bgnd)_{sample}/(Peak - Bgnd)_{std}$ was determined for each of the elements to be analysed using constant beam conditions. The k-values were input to a 'LINK' computer programme based on the ZAF-4 computer programme for ZAF corrections to give the final concentrations. The k-values were also converted into integral intensity ratios by multiplication by the APFs and then input manually to the COR-2 programme to give the true concentrations.

3.2.2. Results of the oxygen and the boron analyses

(a) *FeB and pure B standards.* The WDX oxygen K peak from the Nd-rich boundary phase in the cast $Nd_{15}Fe_{77}B_8$ alloy is shown in fig. 3.

Fig. 2. Backscattered electron image of sintered $Nd_{16}Fe_{76}B_8$.

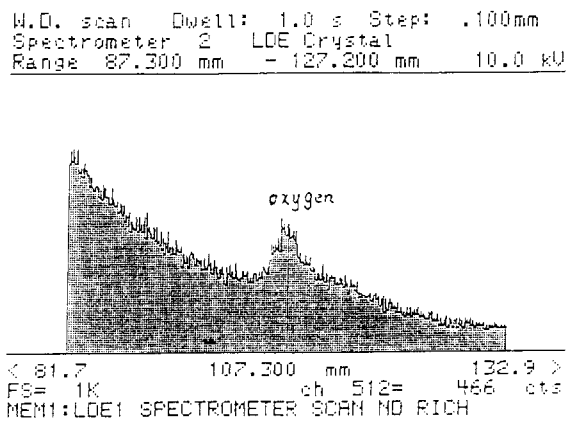

Fig. 3. The WDX oxygen peak in the Nd-rich boundary phase in as cast $Nd_{15}Fe_{77}B_8$.

Boron, oxygen, Nd and Fe contents, and Nd:Fe:B (at%) ratios in the matrix phase, boron-rich phase and Nd-rich phases (including the triple junction region and the $Nd_2Fe_{14}B$–$Nd_2Fe_{14}B$ grain boundaries) obtained via the ZAF-4 program are shown in table 3. Average data were obtained from five independent measurements from each phase.

(b) *Area/peak factors.* Williams [12] recommended that a pure boron standard should be used for experimental convenience. However, pure boron exhibits a much broader boron peak than $Nd_2Fe_{14}B$. The peak shape alterations are very large for B K, but less serious for O K, at least when the LDE crystal is used. The integral intensity measurements can be facilitated by the introduction of the area/peak factor (APF) (the ratio between the true area and the peak intensity for a phase relative to the selected standard) [5]. In this investigation, APFs for B K for the matrix phase and the boron-rich phase in the as-cast $Nd_{15}Fe_{77}B_8$ alloy have been determined with a STE crystal on a JEOL 840A SEM relative to a pure boron standard and are shown in table 4. It is evident that the effects of peak shape alterations for B K are very large indeed and cannot be ignored. Once APFs are available, the peak intensity ratios can be converted easily into

Table 3
Boron and oxygen contents analysed by WDX (10 kV, 5×10^{-8} A), Nd and Fe analysed by EDX using the on-line ZAF-4 programme on a JEOL 840A SEM for the matrix, the Nd-rich and the boron-rich phases. Also given are the total wt%, Nd:Fe:B (at%) ratios and stoichiometric concentrations of the matrix and the boron-rich phases. Error bar = 2×standard deviation.

Standard for B	Phases	Measured concentration (at%)				Total wt%	Nd:Fe:B ratios	Stoichiometric concentration (at%)		
		Nd	Fe	B	O			Nd	Fe	B
Pure boron standard	Matrix phase	11.4 ±0.5	79.3 ±0.6	7.8 ±0.9	1.5 ±0.2	105.0	2:13.9:1.4	11.8	82.4	5.9
	Triple junction region (Nd-rich)	85.4 ±2.0	~1	<1	13.4 ±2.0	94.2				
	Matrix–matrix grain boundary (Nd-rich)	86.5 ±1.6	~1	<1	13.1 ±1.4	95.0				
	Boron-rich phase	10.1 ±0.5	33.9 ±0.5	54.3 ±1.0	1.7 ±1.0	109.8	1:3.3:5.4	12.1	44.0	44.0
FeB standard	Matrix phase	11.9 ±0.4	80.8 ±0.2	5.8 ±1.0	1.5 ±0.2	105.4	2:13.6:1.0			
	Triple junction region (Nd-rich)	85.4 ±0.8	~1	<1	13.4 ±0.1	95.6				
	Matrix–matrix grain boundary (Nd-rich)	85.5 ±2.0	~1	<1	14.0 ±1.3	95.7				
	Boron-rich phase	11.5 ±0.3	39.6 ±0.4	48.2 ±0.2	0.7 ±0.1	107.3	1:3.4:4.2			

Table 4
Area peak factors for the matrix phase and boron-rich phase

	Area of peak (without background) / Height of peak (without background)
Pure boron	30.3 mm
Matrix phase	26.1 mm
Boron-rich phase	23.7 mm
Area/peak factor (APF) for matrix phase, relative to pure boron = 0.8614	
Area/peak factor (APF) for boron-rich phase, relative to pure boron = 0.7822.	

the correct integral intensity ratios by multiplication by the APFs.

(c) *ZAF programmes.* Subsequently, the conversion of the integral intensity ratios into true concentrations depends strongly on the particular ZAF correction programme used and on the quality of the mass absorption coefficients the programme has to work with. Edgley [13] has shown that COR-2 is a more suitable programme to use for quantitative light element analysis. COR-2 may be used with Heinrich's [14] or Henke's [15] mass absorption coefficients for light elements. The integral intensity ratios were then input manually into the COR-2 program (in this study Heinrich's mass absorption coefficients were used) to convert to true concentrations (table 5).

(d) *Mass absorption coefficients (MACs).* Absorption for oxygen K and boron K represents a major part of the correction procedure and the accuracy of the correction depends on an accurate knowledge of the mass absorption coefficients.

A new method has been developed in order to test the accuracy of the existing sets of mass absorption coefficients used in ZAF correction computer programs. The slope of the $I_{\text{oxygen}}/I_{\text{Nd}}$ ratio against foil thickness, which is related to the mass absorption coefficients as shown below, was obtained for pure Nd_2O_3 powder using the convergent beam diffraction technique (for thickness measurements) and ultra-thin window EDX on a JEOL 4000FX TEM.

Figure 4 shows a magnified convergent beam diffraction pattern taken from the pure Nd_2O_3 powder at 400 kV. Fringes within the discs are formed by strongly diffracted beams. The crystal was oriented at a two beam condition: these fringes could be used to determine thickness.

At the same time, ultra-thin window EDX on a JEOL 4000FX TEM was employed to collect oxygen and Nd peaks. The background Bremsstrahlung was subtracted from the obtained spectra of oxygen and Nd by offsetting the cursor on either side of the oxygen and Nd peaks so that the relative intensities of the characteristic X-rays of oxygen and Nd could be determined. The background Bremsstrahlung of the X-ray spectra is proportional to specimen thickness if all the experimental conditions are kept constant. After the thickness of a small area on one Nd_2O_3 particle was determined and the EDX spectrum from this small area was collected, the EDX

Table 5
Boron and oxygen contents analysed by WDX (10 kV, 5×10^{-8} A) using a pure boron standard, Nd and Fe analysed by EDX with the COR-2 programme (Heinrich's MACs) on a JEOL 840A SEM for the matrix, the Nd-rich and the boron-rich phases and Nd:Fe:B (at%) ratios of the matrix phase and boron-rich phase. Error bar = 2×standard deviation.

Phases	Measured concentration (at%)				Nd:Fe:B (at%) ratios
	Nd	Fe	B	O	
Matrix phase	10.6±0.5	82.6±0.5	5.8±0.7	1.0±0.1	2:15.6:1.1
Triple junction region (Nd-rich)	90.4±1.8	~1	<1	8.7±1.9	
Matrix–matrix grain boundary (Nd-rich)	90.6±0.8	~1	<1	8.3±1.0	
Boron-rich phase	11.9±0.5	43.8±0.5	42.9±1.0	1.4±0.1	1:3.7:3.6

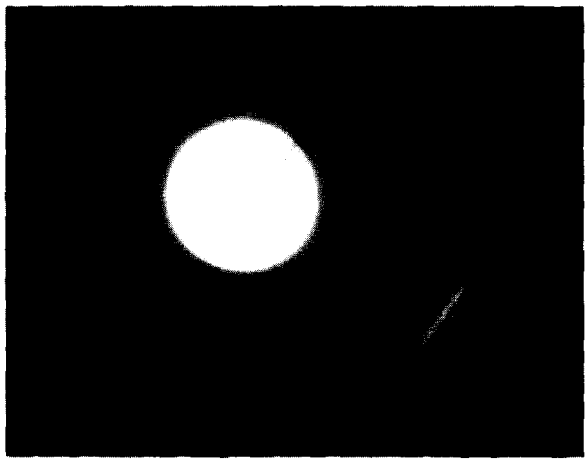

Fig. 4. A magnified convergent beam diffraction pattern (for thickness determination).

spectra of the regions nearby could then be collected. The relative thicknesses of these areas could be determined by comparison of the Bremsstrahlung level. Several groups of data for $I_{\text{oxygen}}/I_{\text{Nd}}$ ratio against specimen thickness were obtained. Figure 5 shows a plot of $I_{\text{oxygen}}/I_{\text{Nd}}$ against specimen thickness. The slope of this curve was approximately 1.1931×10^{-4} Å^{-1} and equals $(\chi_{\text{Nd}} - \chi_{\text{oxygen}})\rho\,|\text{intercept}|/2$. This relation between the slope of the curve and the mass absorption coefficients can be derived by differentiating the equation [16] for quantitative analysis including absorption:

$$I^{\text{abs}}_{\text{Nd}}/I^{\text{abs}}_{\text{oxygen}} = (I_{\text{Nd}}/I_{\text{oxygen}})(\chi_{\text{oxygen}}/\chi_{\text{Nd}}) \times \left[(1 - \exp(-\chi_{\text{Nd}}\rho_{\text{Nd}_2\text{O}_3}t)\right] / \left[(1 - \exp(-\chi_{\text{oxygen}}\rho_{\text{Nd}_2\text{O}_3}t)\right], \quad (1)$$

$$d/dt\left[I^{\text{abs}}_{\text{Nd}}/I^{\text{abs}}_{\text{oxygen}}\right]|_{t=0} = (\chi_{\text{Nd}} - \chi_{\text{oxygen}})\rho\,|\text{intercept}|/2, \quad (2)$$

where

$$\chi_{\text{Nd}} = (\mu/\rho)^{\text{Nd}}_{\text{Nd}_2\text{O}_3} \sin\theta_T/\cos(\theta_T - \theta_E),$$

$$(\mu/\rho)^{\text{Nd}}_{\text{Nd}_2\text{O}_3} = (\mu/\rho)^{\text{Nd}}_{\text{Nd}}C_{\text{Nd}} + (\mu/\rho)^{\text{Nd}}_{\text{oxygen}}C_{\text{oxygen}},$$

$$\chi_{\text{oxygen}} = (\mu/\rho)^{\text{oxygen}}_{\text{Nd}_2\text{O}_3} \sin\theta_T/\cos(\theta_T - \theta_E),$$

$$(\mu/\rho)^{\text{oxygen}}_{\text{Nd}_2\text{O}_3} = (\mu/\rho)^{\text{oxygen}}_{\text{oxygen}}C_{\text{oxygen}}(\text{wt\%}) + (\mu/\rho)^{\text{oxygen}}_{\text{Nd}}C_{\text{Nd}}(\text{wt\%}),$$

$\theta_T = 60°$, $\theta_E = 0°$ (see fig. 6);

ρ is the density of the Nd_2O_3 powder, for hexagonal 7.31 g/cc and for cubic 6.6 g/cc [17].

After inputting Heinrich's [14] and Henke's [15] mass absorption coefficient data, the results are listed in table 6. It can be seen that the experimental data from the pure Nd_2O_3 powder

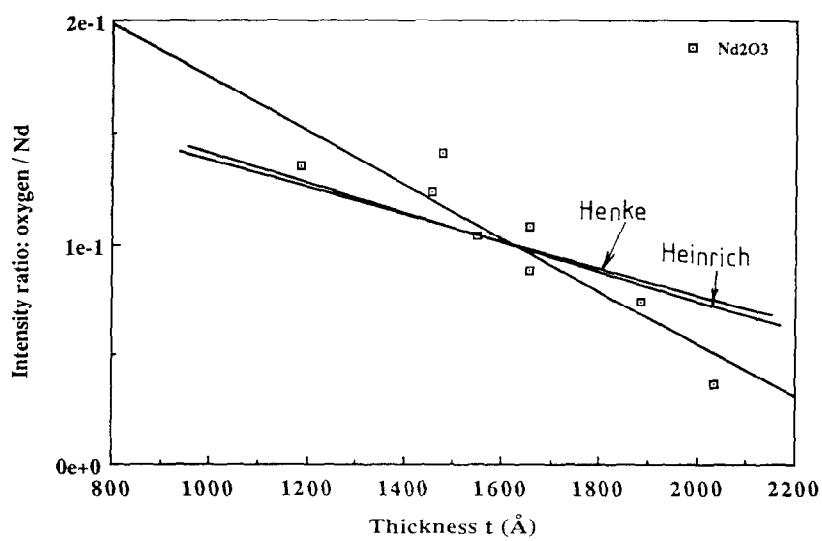

Fig. 5. A plot of $I_{\text{oxygen}}/I_{\text{Nd}}$ ratio against specimen thickness with Heinrich's [14] and Henke's [15] data superimposed.

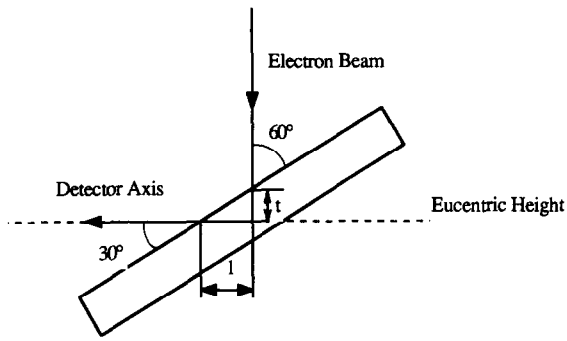

Fig. 6. The specimen and the ultra-thin window EDX detector geometry in the JEOL 4000FX TEM. t, X-ray generation depth; l, average X-ray path length. The angle θ_T between the electron beam and the specimen is here 60°, and the angle θ_E above the horizontal of the detector is here 0°.

are higher than the theoretical values of Heinrich and Henke but they are reasonably close. This gives us some confidence in the mass absorption coefficients which are widely used in the ZAF correction computer programme.

The integral intensity ratios were corrected with the COR-2 program again using the mass absorption coefficient of oxygen by Nd measured in this work to convert into true concentrations (table 7).

(e) *Applications.* The results (table 5) show clearly that the triple junctions and the $Nd_2Fe_{14}B$–$Nd_2Fe_{14}B$ grain boundaries in the cast $Nd_{15}Fe_{77}B_8$ alloy contain the Nd-rich phase and they have composition:

Nd ~90 at%, Fe: ~1 at%,
oxygen: 8–9 at%, boron: <1 at%.

The amount of oxygen was found to be fairly low ~1 at% in the matrix and boron-rich phases (presumably an oxide film).

Turning to the sintered specimen, Nd, Fe, boron and oxygen contents at the centres of matrix grains derived from the ZAF-4 program are shown in table 8. An FeB standard for boron was used. There is only ~1.7 at% oxygen in the matrix phase. Average data come from five independent measurements.

The capability of WDX spectrometry for light element analysis is somewhat limited by its low spatial resolution. It is very difficult or even impossible for the electron probe beam to resolve down to 1 μm. Furthermore, the volume of the

Table 6
Comparison of the experimental data with those of Heinrich [14] and Henke [15] (*Note*: for hexagonal Nd_2O_3, the density $\rho = 7.31$ g/cc and for cubic Nd_2O_3, the density $\rho = 6.6$ g/cc)

	$\rho(\chi_{oxygen} - \chi_{Nd})\lvert\text{intercept}\rvert/2$ (Å^{-1})		oxygen $(\mu/\rho)_{Nd}$ (cm^2/g)	
	Hexagonal Nd_2O_3	Cubic Nd_2O_3	Hexagonal Nd_2O_3	Cubic Nd_2O_3
Experimental data	1.19×10^{-4}		7569	8374
Heinrich [14]	0.98×10^{-4}	0.88×10^{-4}	6216	
Henke [15]	0.89×10^{-4}	0.81×10^{-4}	5690	

Table 7
Using $(\mu/\rho)_{Nd}^{oxygen}$ from this work, boron and oxygen contents of the Nd-rich phase analysed by WDX (10 kV, 5×10^{-8} A) using a pure standard on a JEOL 840A SEM. Error bar = 2×standard deviation

Phases		Measured concentration (at%)			
		Nd	Fe	B	O
Triple junction region (Nd-rich)	$(\mu/\rho)_{Nd}^{oxygen} = 7569$ cm^2/g	90.5±1.9	~1	<1	8.7±1.9
Matrix–matrix grain boundary (Nd-rich)		91.4±1.2	~1	<1	8.3±1.0
Triple junction region (Nd-rich)	$(\mu/\rho)_{Nd}^{oxygen} = 8374$ cm^2/g	89.0±2.1	~1	<1	10.2±2.2
Matrix–matrix grain boundary (Nd-rich)		90.1±1.3	~1	<1	9.7±1.1

sample which contributes to the X-ray signal is relatively independent of the size of the electron probe because high angle elastic scattered electrons within the sample generate X-rays. These factors together limit the application of WDX in obtaining further information from the Nd-rich and boron-rich boundary phases along the grain boundaries in this sample, which has a very fine grain size (see fig. 2).

3.3. Auger Electron Spectroscopy

The escape depths (the distance over which the X-ray energy will reduce to an arbitrary fraction, for example, 50%) of the X-rays for boron and oxygen are of the order of 100 nm (for example, the calculated escape depths of the X-rays for boron in $Nd_2Fe_{14}B$ and oxygen in Nd_2O_3 in the present work are ~28 and ~120 nm respectively) and the accuracy of the results is then sensitive to the surface conditions of the specimen.

The presence of oxygen in the Nd-rich grain boundary phase and the specimen surface was confirmed by Auger spectroscopy. Figure 7 shows the elemental distributions determined by Auger spectroscopy from the matrix phase, Nd–O boundary phase and boron-rich phase in the homogeneous $Nd_{15}Fe_{77}B_8$ alloy. There are several points of interest in these spectra. First, there was serious carbon contamination on the surface. Second, there was a large amount of oxygen present. Third, there was no detectable boron in these three phases, the matrix phase was Fe-rich and the Nd–O boundary phase was Nd-rich.

After ion etching for 15 min, the Auger spectra were collected again from these three phases. The Auger spectra are shown in fig. 8. Depth profiling of the sample revealed several interesting points. First, the surface carbon contamination disappeared. Second, the oxygen signal decreased significantly in the matrix phase and the boron-rich phase. Third, the oxygen present in the Nd–O boundary phase did not change with depth. Fourth, there was detectable boron in the boron-rich phase. Finally, at the low-energy left end of the Auger spectra, Nd and Fe Auger peaks appeared. These results indicate that the large amount of oxygen present in the matrix phase and in the boron-rich phase existed predominantly in the surface layer.

4. Discussion

A successful analysis of light elements using WDX on a SEM involves specimen preparation, intensity measurements and ZAF correction. For specimen preparation, any non-recently prepared specimens would have excess surface oxidation. For intensity measurements, the major problem is the very low count rates and low peak to background ratios. In the present studies, a LDE-1 crystal (for the quantitative analysis of oxygen) is introduced to produce much higher peak intensities. Large errors in the intensity measurements can be made when peak shape alterations (exact peak position can vary with valency state) are ignored, especially for boron.

Since the boron content obtained by the use of an FeB standard is closer to the stoichiometric concentration of the matrix phase, it can therefore be concluded that the FeB standard is more appropriate than the pure boron standard al-

Table 8
In sintered $Nd_{16}Fe_{76}B_8$, boron and oxygen contents analysed by WDX (10 kV, 5×10^{-8} A), Nd and Fe analysed by EDX with the on-line ZAF-4 programme on a JEOL 840A SEM, and Nd:Fe:B (at%) ratios for the matrix phase

Sample name	Phases	Measured concentration (at%)				Nd:Fe:B (at%) ratio
		Nd	Fe	B	O	
Laboratory-produced sintered $Nd_{16}Fe_{76}B_8$ magnet (FeB standard for boron analysis)	Matrix phase	12.8 ± 0.9	79.2 ± 1.0	6.3 ± 0.1	1.7 ± 0.1	2:12.4:1.0
	Low spatial resolution of WDX prevented analysis of the grain boundary region					

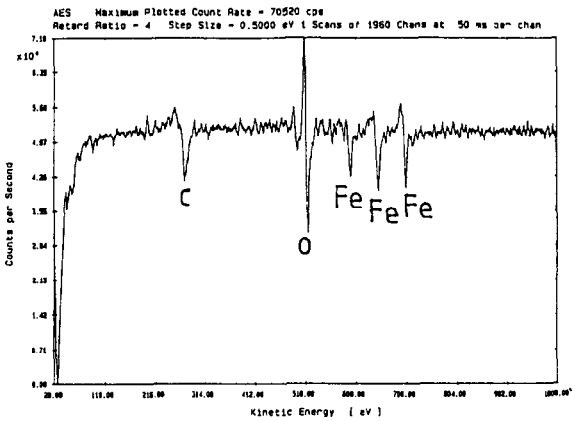

matrix

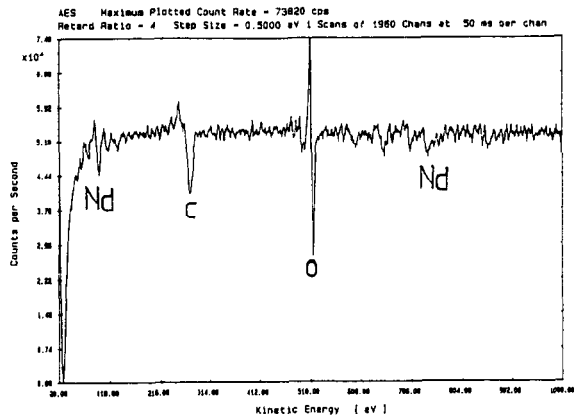

Nd-rich

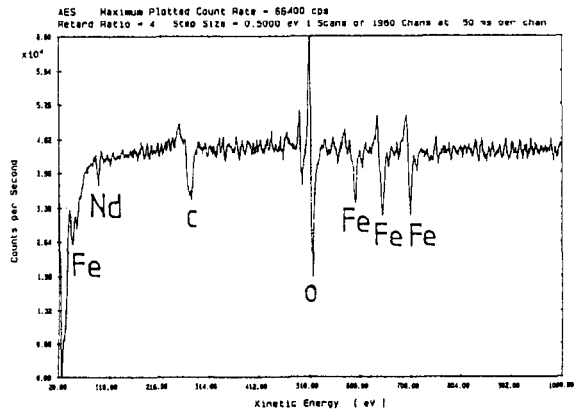

Boron-rich

Fig. 7. Auger spectra from three phases before ion etching.

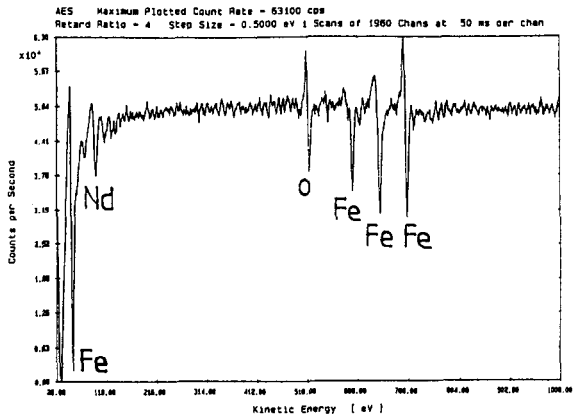

matrix

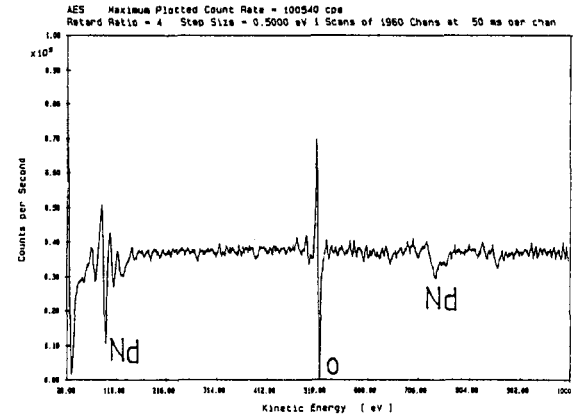

Nd-rich

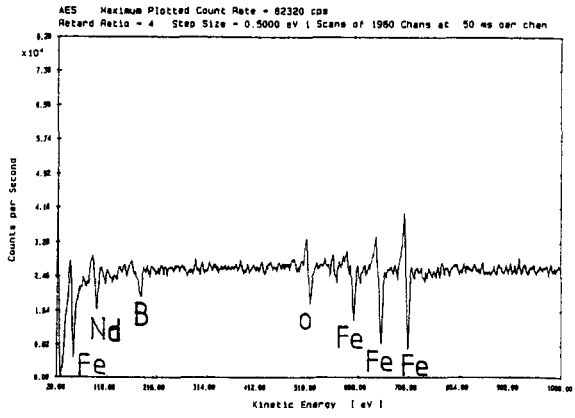

Boron-rich

Fig. 8. Auger spectra from three phases after 15 min ion etching.

though the measured boron content must be lower than the exact boron content in the phases because of the absorption of boron by the surface contamination. Structure determination by selected area diffraction in the TEM [18] confirmed that the matrix phase has a tetragonal structure with c/a ratio identical to that determined by neutron diffraction [19] and therefore the matrix phase was concluded to be $Nd_2Fe_{14}B$. The homogeneity range in $Nd_2Fe_{14}B$ is either absent or very small. This was determined from the small variations in the lattice constants [20] or the Curie temperature, which lies in the range 581–584 K [21]. These indicate that there is probably only one possible composition. The $Nd_{(1+\epsilon)}Fe_4B_4$ compound is characterised as a member of the composition-modulated structural series $R_{(1+\epsilon)}Fe_4B_4$ (R = Ce, Pr, Nd, Sm, Gd, Tb) with variable R content [0.11 (Pr) $\leq \epsilon \leq$ 0.15 (Tb)] [22]. The reason for the improvement in boron measurements could be attributed to the fact that the FeB standard is closer to the composition within the magnetic alloys and the shape of the peak produced from the FeB standard is more similar to those from the matrix phase and the boron-rich phase than that of the pure boron standard. The results might be improved further by using even closer composition standards.

However, for experimental convenience, a pure boron standard should be used [12]. The peak shape alterations could be compensated by the introduction of the area/peak factors. Accuracy in boron measurements has been improved after the introduction of APFs for boron and the employment of the COR-2 programme with Heinrich's mass absorption coefficients. The phase at the $Nd_2Fe_{14}B$-$Nd_2Fe_{14}B$ grain boundaries and three grain junctions had the same composition ($\sim$ 90 at% Nd, $\sim$ 1 at% Fe, 8–9 at% oxygen and $<$ 1 at% boron) suggesting that the $Nd_2Fe_{14}B$–$Nd_2Fe_{14}B$ grain boundary region is an extension of the phase from the triple-point region. The oxygen composition measured by WDX in this work (COR-2 programme) is lower than published data estimated by EPMA on the fcc Nd-rich phase with a = 0.52 nm which has 80–85 at% Nd, 2–3 at% Fe, balance oxygen [23] although in the present case, TEM diffraction patterns showed that the Nd-rich phase has a fcc (a = 0.52 nm) + complex bcc (a = 1.04 nm) structure [18]. This phase was stabilised by a significant amount of oxygen (8–9 at% oxygen). The published data are, however, very close to the data obtained from the ZAF-4 programme, which may not be reliable.

Regarding the results for oxygen, previous authors [8] showed that oxygen contamination in WDX is almost as serious a problem as carbon contamination. Carbon contamination could be reduced by placing a 'cold finger' near the surface of the sample. The former effect is much more difficult to combat than the latter due to the relatively poor vacuum conditions in commercial WDX systems. Therefore, the accuracy of the measured oxygen in the sensitive Nd-rich phase is still open to doubt.

Regarding the ZAF correction, absorption represents the major part. It is vital that mass absorption coefficients are available with an accuracy of $\pm$ 1%. The result by Bastin [8] indicated that it is more likely that the poor analyses are caused by inaccuracy in the published mass absorption coefficients than by inadequacies in the correction programmes themselves. However, the inadequacies in the models used in the correction programme may also be a problem. For example, the Philibert absorption correction model [2,24] assumes that Φ_0 (the value of the depth distribution of generated characteristic X-rays $\Phi(\rho Z)$ at the surface) = 0 and this is not acceptable for soft X-rays.

In the present work, the mass absorption coefficient of oxygen by Nd was measured from pure Nd_2O_3 powder using a convergent beam technique (for thickness measurement) and ultra-thin window EDX on a JEOL 4000FX TEM. It can be seen from fig. 5 that the agreement between the experimental line and the theoretical lines [14,15] is reasonably good. This implies that the variation of $I_{\text{oxygen}}/I_{\text{Nd}}$ intensity ratio with thickness is a satisfactory straight line (correlation coefficient = 91.4%). The results as shown in table 6 suggest that the mass absorption coefficients estimated using this method are reasonably close to the value used in the COR-2 computer programme for the ZAF correction. It is also interesting to

note that the experimental data are closer to Heinrich's data than Henke's data, which is in agreement with the measurements of Edgley [13]. The use of $(\mu/\rho)_{Nd}^{oxygen}$ from this work in COR-2 made oxygen concentrations slightly higher than those obtained via Heinrich's data.

The accuracy of the measured boron and oxygen is very sensitive to the surface conditions. This can be seen from the Auger spectroscopy. The Auger spectra before the ion depth profiling suggested that there was serious carbon contamination on the surface together with a large amount of oxygen. This serious carbon contamination will reduce the signals from Nd, Fe, oxygen and boron. The large amount of oxygen must include the effect of surface oxidation. The previous work by Fujii et al. [25] using small-angle neutron scattering and Elbicki et al. [26,27] using Auger spectroscopy suggested that the surfaces of the grains in Nd–Fe–B magnets are rich in Nd and oxygen but poor in Fe. They suggested that the surfaces of the grains are nonmagnetic and called them magnetic dead layers. They also concluded that this surface shell of dead layers insulates one grain from another and could generate significantly large coercivity. They further attributed the improvement of coercivity by post sintering heat treatment to formation of a more uniform distribution of magnetic dead layers over the grains. From the present investigation, this so-called '~ 50 Å magnetic dead layer' is probably only the Nd-rich grain boundary phase. During depth profiling, the oxygen signal in the matrix grains and boron-rich grains decreases significantly. The Nd, Fe and boron signals, which were absorbed by the oxygen rich surface layer, increased relatively. The oxygen signal in the Nd-rich boundary phase did not change after depth profiling suggesting that the oxygen reacted with the Nd-rich boundary phase to form a bulk Nd oxide because of the large affinity of the Nd for oxygen.

5. Conclusions

(1) Analyses of boron and oxygen were carried out using WDX. The conditions for the WDX measurements including the proper standards, accelerating voltage, probe current and crystals employed for boron and oxygen have been described. Excellent concentration reproducibility has been achieved in our experiments. Accuracy in boron measurements has been achieved (using a pure boron standard) with the introduction of the APFs and the COR-2 programme although the results for boron with the ZAF-4 program can be improved using an FeB standard rather than the pure boron standard. The Nd-rich phase has ~ 90 at% Nd, ~ 1 at% Fe, 8–9 at% oxygen and < 1 at% boron. The amount of oxygen was found to be fairly low (~ 1 at%) in the matrix and boron-rich phases. The low spatial resolution of WDX limits its application in obtaining further information on the boundary phases in the laboratory HD-produced sintered magnet, which has a very fine grain size.

(2) A novel method has been developed to measure mass absorption coefficients.

(3) Auger spectroscopy results show that the large oxygen concentration present in the matrix phase and in the boron-rich phase only existed in the surface layer but by contrast the oxygen reacted with the Nd-rich boundary phase to form a bulk Nd oxide.

Acknowledgements

The authors would like to thank Mr D.S. Edgley for his help in using the COR-2 programme and many useful suggestions. Thanks are due to the Science and Engineering Research Council (SERC) and to Concerted European Action on Magnets (CEAM) for support of the general research programme of which this work forms a part. One of the authors (X.J. Yin) is grateful to the British Council and the Chinese State Education Commitee for financial support.

References

[1] M.G. Hall, Wavelength Dispersive X-ray Analysis, Internal Report, School of Metallurgy and Materials, University of Birmingham, UK (1990).

[2] S.J.B. Reed, Electron Microprobe Analysis (Cambridge University Press, Cambridge, 1975).
[3] G.F. Bastin and H.J.M. Heijligers, X-ray Spectrometry 15 (1986) 135.
[4] G.F. Bastin and H.J.M. Heijligers, in: Microbeam Analysis, ed. P.E. Russell (1989) p. 207.
[5] G.F. Bastin and H.J.M. Heijligers, Scanning 12 (1990) 225.
[6] J. Henoc, K.F.J. Heinrich and R.L. Myklebust, National Bureau of Standards (US), Tech. Note 769 (1973).
[7] R.L. Myklebust, K.F.J. Heinrich and H. Yakowitz, National Bureau of Standards (US), Tech. Note 796.
[8] G.F. Bastin and H.J.M. Heijligers, in: Microbeam Analysis, ed. D.E. Newbury (1988) p. 325.
[9] I.R. Harris, J. Less-Common Metals 131 (1987) 245.
[10] P.M. Kelly, A. Jostsons, R.G. Blake and J.G Napier, Phys. Stat. Solidi. (a)31 (1975) 771.
[11] D.C. Joy and J.P. Jakubovics, Phil. Mag. 145 (1968) 61.
[12] A.J. Williams, Application of light element analysis to studies of Nd–Fe–B magnetic materials, Third year project, School of Metallurgy and Materials, University of Birmingham, UK (1990).
[13] D.S. Edgley, Application of light element analysis to studies of rare-earth/boron magnetic materials, Third year project, School of Metallurgy and Materials, University of Birmingham, UK (1991).
[14] K.F.J. Heinrich, X-ray Optics and Microanalysis, 11th Int. Congr., University of Western Ontario (1987) 67.
[15] B.L. Henke, P. Lee, T.J. Tanaka, R.L. Shimabukuro and B.K. Fujikawa, Atomic Nucl. Data Tables 27 (1982) 1.
[16] M.H. Loretto, Electron Beam Analysis of Materials (Chapman and Hall, London, 1984) p. 160.
[17] K. Gschneider Jr, Rare Earth Alloys (Los Alamos, New Mexico, 1960).
[18] X.J. Yin, PhD Thesis, University of Birmingham, UK (1992).
[19] J.F. Herbst, J.J. Croat, P.E. Pinkerton and W.B. Yelon, Phys. Rev. B29 (1984) 4176.
[20] H.H. Stadelmaier, N.A. El-Masry, N.C. Liu and S.F. Cheng, Mater. Lett. 2 (1984) 411.
[21] K.H.J. Bushow, D.B. de Mooij and H.M. Van Noort, Philips J. Res. 40 (1985) 277.
[22] A. Bezinge, H.F. Braun, J. Muller and K. Yvon, Solid State Commun. 55 (1985) 131.
[23] D. Cochet-Muchy and S. Paidassi, in: CEAM Report, ed. I.V. Mitchell et al. (Elsevier Applied Science, Amsterdam, 1989) 369.
[24] K.F.J. Heinrich and D.E. Newbury, Electron Probe Quantization (Plenum Press, New York, 1991).
[25] H. Fujii, T. Takeda, S. Kamura, T. Okamoto, S. Hirosawa and M. Sagawa, IEEE Trans. Magn. MAG-23 (1987) 3119.
[26] J.M. Elbicki, W.E. Wallace and P. Wynblatt, J. Magn. Magn. Mater. 74 (1988) 186.
[27] J.M. Elbicki, W.E. Wallace and V. Korablev, IEEE Trans. Magn. 25 (1989) 3567.